Fiber-detector subsystem loss comparison for a ground-based photon-counting optical receiver

Brian E. Vyhnalek and Sarah A. Tedder

National Aeronautics and Space Administration
Glenn Research Center
Cleveland, OH, USA

ABSTRACT

In this paper we present a comparative study of the losses associated with fiber-coupled single-photon detectors in two different configurations, each with the goal of receiving a pulsed-position modulated signal with a maximum data rate of 267 Mbps. First, we consider a 7x1 few-mode-fiber (FMF) photonic lantern coupled to seven individual superconducting nanowire single photon detectors (SNSPDs). In the second configuration we assess a single FMF coupled to a 16-channel monolithic SNSPD array. In each case we measure and compare combined fiber coupling, SNSPD blocking, and system efficiency losses under emulated atmospheric turbulence conditions. We address subsystem impact on link performance and analyze feasibility for future NASA lunar and deep-space optical communications missions.

Keywords: Optical communications, photonic lantern, single photon detectors, few-mode fibers

1. INTRODUCTION

For free-space optical communications links on photon-starved channels in which power efficiency is the main constraint on link design, such as lunar-to-ground or deep space missions, capacity-approaching serially-concatenated pulse-position modulation (SCPPM),[1] along with critical technologies such as single photon detectors featuring high efficiency, high count rate, low dark counts and low jitter provide the necessary basis on which to develop highly sensitive ground-based receiver systems. The SCPPM format is part of the Consultative Committee for Space Data Systems (CCSDS) recommended Optical Communications High Photon Efficiency (HPE) Standard,[2] which is planned for the upcoming NASA Orion Artemis-2 Optical Communications demonstration from lunar distances,[3] and the Deep Space Optical Communications (DSOC) Project whose optical transciever will be hosted aboard the Psyche Mission spacecraft out to distances greater than 2 AU.[4,5] In both cases the ground receiver segment will be based on single-photon counting systems.

While SCPPM's capacity-approaching modulation and forward-error correction scheme, along with high efficiency and high timing resolution single-photon counting detectors are the key underlying technologies to enable power constrained links, additional considerations must be given to the optical interconnects between the receiver telescope and detectors. Particularly under conditions of atmospheric turbulence, in which the propagating beam is distorted into a multi-moded spatial profile, significant losses can be suffered in the receiver

Send correspondence to brian.e.vyhnalek@nasa.gov

system at the interface behind the telescope. In light of this, we have investigated coupling losses into several different fiber interconnects, namely graded-index few-mode and multi-mode fibers, single-mode and few-mode photonic lanterns, and a few-mode multi-plane light conversion (MPLC) device with emulated atmospheric turbulence.[6–8] Here we again explore the effect of atmospheric turbulence on fiber interconnects, but now include measurements of the count rate distributions at the single photon level. However, we restrict the analysis to only the few-mode photonic lantern and single FMF. With these measurements in combination with the total fiber insertion loss and single-photon detector blocking losses, we determine the overall fiber-detector subsystem efficiencies for different levels of turbulence and received power. Finally, we assess link performance implications.

2. RECEIVER DESCRIPTION

The HPE-compatible optical communications receiver under development at the NASA Glenn Research Center consists of a fiber interconnect, which couples a receiving telescope aperture to detectors, superconducting nanowire single photon detectors (SNSPDs), and a field programmable gate array (FPGA) receiver modem[9] for real-time single photon counting. Individual SNSPDs are in principle capable of count rates on the order of 10 Gcps, but due to kinetic inductance effects can practically achieve count rates into the 10s of Mcps,[10] hence in order to reach higher data rates multiple detectors must be used in parallel. Accordingly, we have explored the two fiber-detector architectures described next, based around commercially available SNSPDs.

2.1 Photonic Lantern to Individual SNSPDs

Depicted in Figure 1 is the first fiber-detector subsystem architecture considered, based on a FMF photonic lantern and individually fiber coupled SNSPDs. The SNSPDs are commercial devices, with typical meander nanowire geometries, approximately 14 μm in diameter, and operating temperature of 2.5 K in a rack-mounted cryocooler. The nominal highest detection efficiency operating wavelength is centered at 1550 nm, with an approximate 10% efficiency reduction across the optical C-band. Electrically, the SNSPDs are current biased with a DC-coupled preamplifier stage, and readout through room temperature low-noise amplifiers, with gain on the order of 50 dB at 500 MHz bandwidth.

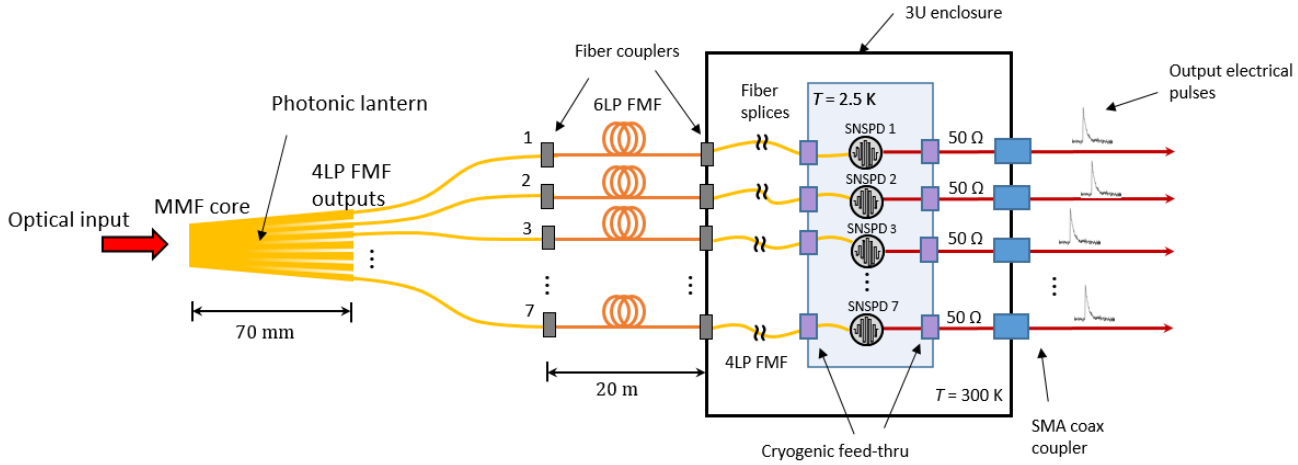

Figure 1: Schematic of the 1 × 7 photonic lantern coupled SNSPD subsystem.

Typically, commercial SNSPDs at 1550 nm are fiber-coupled to single-mode SMF-28 fiber. However, in our system we fiber couple to 20-μm graded-index (GRIN), 0.19 NA core few-mode fiber (FMF), supporting the modes $LP_{01}, LP_{11e}, LP_{11o}, LP_{21e}, LP_{21o}$ and LP_{02} for a total of 6 propagating modes, not including polarization. Due to the index grading, the 20-μm FMF has similar mode field sizes to SMF-28, hence can be coupled to standard SNSPDs with minimal mode-dependent coupling loss.[11] From Figure 1 we see that the fibers directly

coupled to the SNSPDs are then sent through a cryogenic vacuum feed-thru panel before being spliced to fibers connectorized to the front of a 3U enclosure. Measured dark count rates with the front panel ports capped were initially on the order of 10-30 kcps when biased for 80%-82% detection efficiency, but have subsequently been reduced by a factor of 10× or so with the addition of AR coatings to the end faces of the fibers coupled to the SNSPDs.[11,12]

On the input side, light is coupled from the receive telescope through a focusing lens into a photonic lantern. In most applications a photonic lantern features several single-mode output fibers fused and tapered into a multi-moded input, sized such that the number of supported input modes equals the number of output single-mode fibers. However, for efficient coupling through turbulence a large number of modes is desired, which would in turn require many SMF outputs and hence SNSPDs. Our solution, previously described[6–8] has been to develop a photonic lantern based on FMF to reduce the number of detectors. To this end, we have fabricated a 1×7 photonic lantern with a multi-moded input core approximately 55 μm in diameter, seven 6-mode FMF outputs, with a taper length of 70 mm, for a total coupling of 42 input modes. Since the output FMF of the photonic lantern are relatively short, we separately couple each output to additional FMF[13] (6LP, 10-mode, < 0.5 dB loss coupling to 4LP FMF), 20 m each in length, to the input ports on the SNSPD enclosure, for practical deployment.

2.2 Few-Mode Fiber to Multi-Element SNSPD Array

As an alternative architecture, depicted in Figure 2, we reduce the complexity of the fiber interconnection by increasing the complexity of the detector, in this case coupling a single to a multi-detector SNSPD array. The SNSPD array is commercially fabricated[14] and consists of 16 sub-elements, 16 μm $\times$ 1 μm, in a linear configuration for a total device size of 16 μm $\times$ 16 μm. Unlike interleaved SNSPD arrays, such as used for NASA's Lunar Laser Communications Demonstration (LLCD),[15] the linear array configuration provides 1-D spatial information of the light distribution incident on the detector. As before, the graded-indexing on the input 4LP, 6-mode FMF allows for nearly lossless coupling to the SNSPD. For the fiber interconnect from the front panel of the SNSPD enclosure to the optical input, we use a 6LP, 10-mode FMF fiber as mentioned above. The initial system design was for identical fiber for coupling to the SNSPD array and telescope. However, due to challenges in obtaining the required quantities we opted to use a more readily available FMF with a slightly larger core.

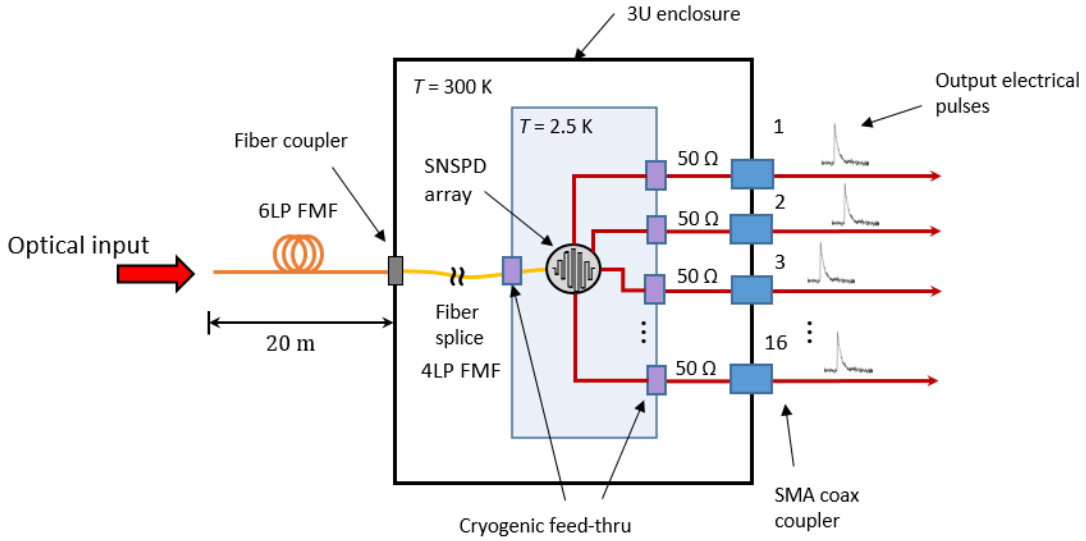

Figure 2: Schematic of the FMF coupled 16-channel SNSPD array subsystem. Although shown separately from Figure 1 for illustration, the SNSPD array is physically mounted to the same cold head as the 7 single element SNSPDs coupled to the photonic lantern.

The detector sub-elements of the SNSPD array are each individually wired for separate biasing and output amplification, using the same electronics as for the single element devices. From device characterization,[14] typical dark count rates per detector are on the order of 3 - 10 kcps, with a composite array system detection efficiency (SDE) of $SDE \approx 83\%$. Detection jitter is similar to the single-element devices, about 75 – 95 ps FWHM, however the average $1/e$ reset time is $\tau_{array} \approx 9$ ns, about half the single element reset time of $\tau_{single} \approx 15 - 18$ ns, implying a greater potential for higher-rate communications applications.

3. EXPERIMENTAL SETUP

Previously we have separately measured losses associated with the individual receiver subsystem components, in particular the total coupling loss of the photonic lantern and FMF using emulated atmospheric turbulence,[6–8] as well as SNSPD detection efficiency and flux-dependent blocking losses.[11,12,16] An additional important consideration is the loss due to the potentially non-uniform intensity distribution across the detectors under different turbulence conditions. A non-uniform intensity distribution could increase blocking losses, particularly for higher rate applications as certain detectors could be preferentially illuminated and driven into saturation.

We quantify the additional loss in both systems by using the NASA Glenn Research Center's Arbitrary Light Field Generator (ALF-G), depicted in Figure 3. This system has been described in detail elsewhere,[17,18] but we will summarize the salient features here. As shown in Figure 3, a linearly polarized fiber-coupled 1550 nm laser is collimated with an 80 mm focal length collimator to form a 14.5 mm diameter beam. A half-wave plate (HWP) rotates the polarization to align the sensitive axis of a liquid crystal spatial light modulator (SLM). The SLM has 1920 × 1200 active liquid crystal elements, with 8 μm pixel pitch, comprising a total 15.36 × 9.6 mm surface area. Each element has 10-bit depth, corresponding to 1024 phase levels from 0 to 2π.

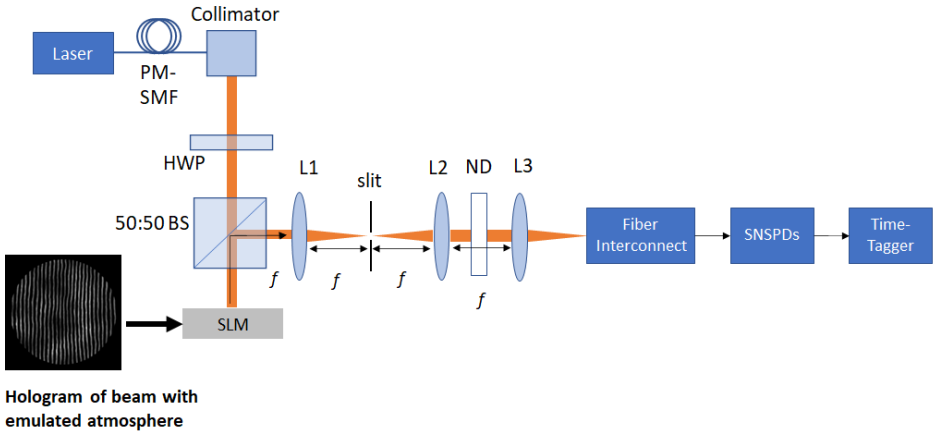

Figure 3: Schematic of the experimental setup.

The light incident on the SLM is modulated using a complex-amplitude phase hologram to emulate a beam after propagation through the atmosphere,[7,19] and then is reflected off the SLM and back through BS1 along the second path. A circular aperture was emulated on the SLM by defining phase holograms truncated to a diameter set to 66.5% of the linear dimension of the central 1200 × 1200 pixel active area of the SLM corresponding to a 6.4 mm pupil. A $4f$ system relays the optical field at the SLM plane to the plane of L3, after which the modulated light is focused into either the photonic lantern or FMF. Between L1 and L2 we use a spatial filter to remove higher diffraction orders created by the grating of the hologram. Addtionally, between L2 and L3 we insert ND filters to attenuate the input signal to single photon levels. After detection by the SNSPDs the outputs of each channel are sent to a high resolution time-tagging unit to record count rates.

4. RESULTS

4.1 Receiver Channel Detection Uniformity

We measured the per-channel photon count rates for the two receiver subsystems for a range of turbulence conditions, parameterized by the ratio of the receiver aperture diameter to Fried's atmospheric coherence diameter, D/r_0, for $D/r_0 = \{2, 4, 6, 9, 15, 20, 30\}$. We selected different coupling lenses, L3 in Figure 3, to note the effect of coupling lens NA on the count rate distributions. It has been shown[6,20] that the optimal NA is a function of D/r_0, with more sensitivity shown by the photonic lantern, compared to a single FMF. For the photonic lantern (PL) subsystem we used $\mathrm{NA}_{PL} = \{0.064, 0.10, 0.16\}$ and for the FMF-SNSPD array system we used $\mathrm{NA}_{FMF} = \{0.16, 0.18, 0.21\}$. Since the SLM modulation rate is well below the rate of atmospheric turbulence, we use 100 different realizations of turbulent spatial profiles for each D/r_0 to statistically assess the count rate distributions. Figures 4-6 show the normalized count rate distributions, averaged over the 100 different spatial inputs, for the various D/r_0.

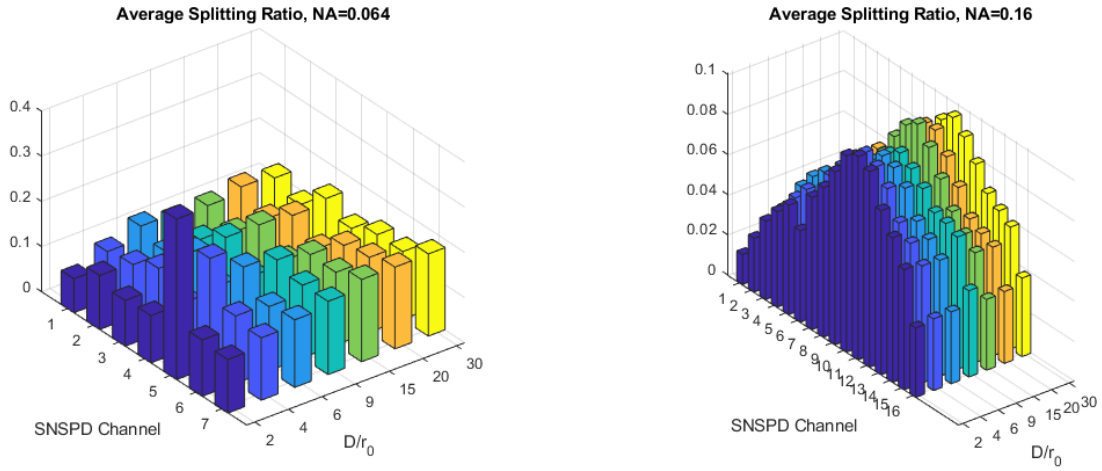

(a) (b)

Figure 4: (a) Photonic lantern+7 single SNSPDs normalized count rates with input NA = 0.064. (b) FMF+16-channel SNSPD array normalized count rates with input NA = 0.16.

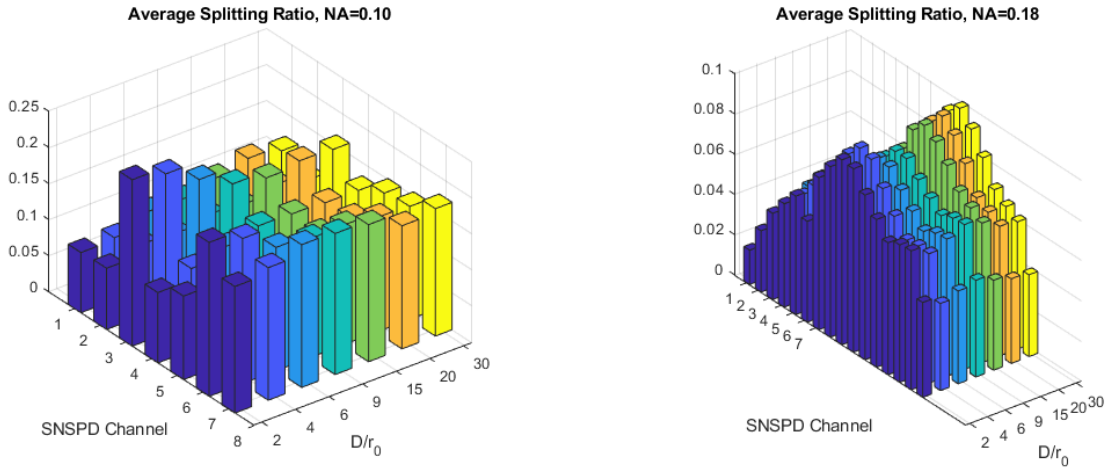

(a) (b)

Figure 5: (a) Photonic lantern+7 single SNSPDs normalized count rates with input NA = 0.10. (b) FMF+16-channel SNSPD array normalized count rates with input NA = 0.18.

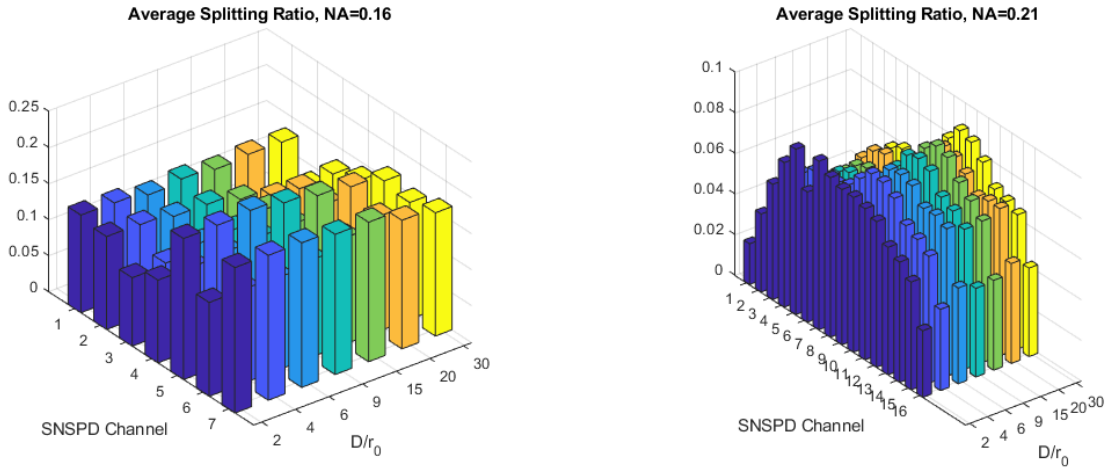

(a) (b)

Figure 6: (a) Photonic lantern+7 single SNSPDs normalized count rates with input NA = 0.16. (b) FMF+16-channel SNSPD array normalized count rates with input NA = 0.21.

As can be observed in Figures 4-6, there appears to be greater non-uniformity of the count distributions for the photonic lantern system for different NA, and variation with D/r_0. To simplify the presentation of these dependencies, we calculate the variance across detector channels as a function of D/r_0, and plot these results in Figure 7 for different NAs. In Figure 7 it can be seen that for all configurations, the count rate non-uniformity is less than 10%. For the photonic lantern system, there is the most channel count non-uniformity for NA=0.064 and $D/r_0 = 2$ (blue stars). However, for $D/r_0 > 2$, the deviation drops significantly and for $D/r_0 > 4$, this configuration has the least non-uniformity for the photonic lantern based system. The FMF system had lower deviation overall, around 2-2.5%, with minimal dependence on D/r_0. In the next section we quantify the input light non-uniformity effect on detector blocking loss.

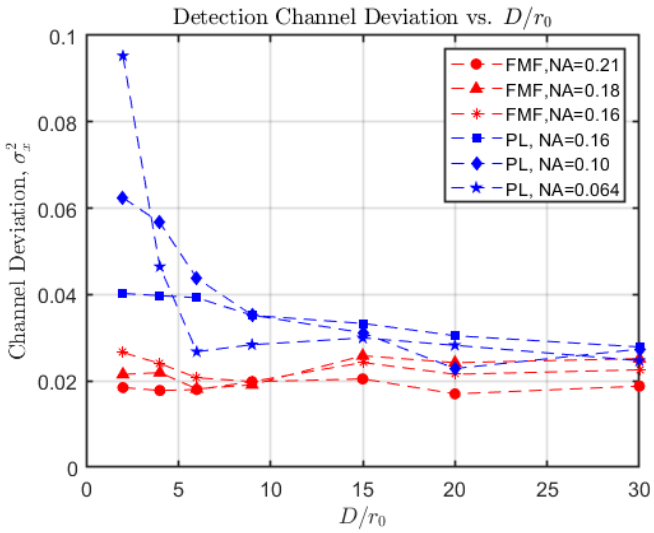

Figure 7: Detection uniformity deviation across detector channels. Dotted lines are visual guides.

4.2 Subsystem Loss Analysis

In this section we analyze the total fiber-detector subsystem losses under different turbulence conditions and over a range of received power, combining the overall fiber coupling losses with SNSPD blocking and input light distribution non-uniformity. In Figure 8a we show the total average coupling loss through the different fiber interconnects for D/r_0 up to $D/r_0 = 10$, for optimal NA.[7] This is the nominal range of expected turbulence for NASA's Low Cost Optical Terminal site.[21] Figure 8b shows the average blocking losses for the single element SNSPDs and 16-channel array, as a function of input photon flux.

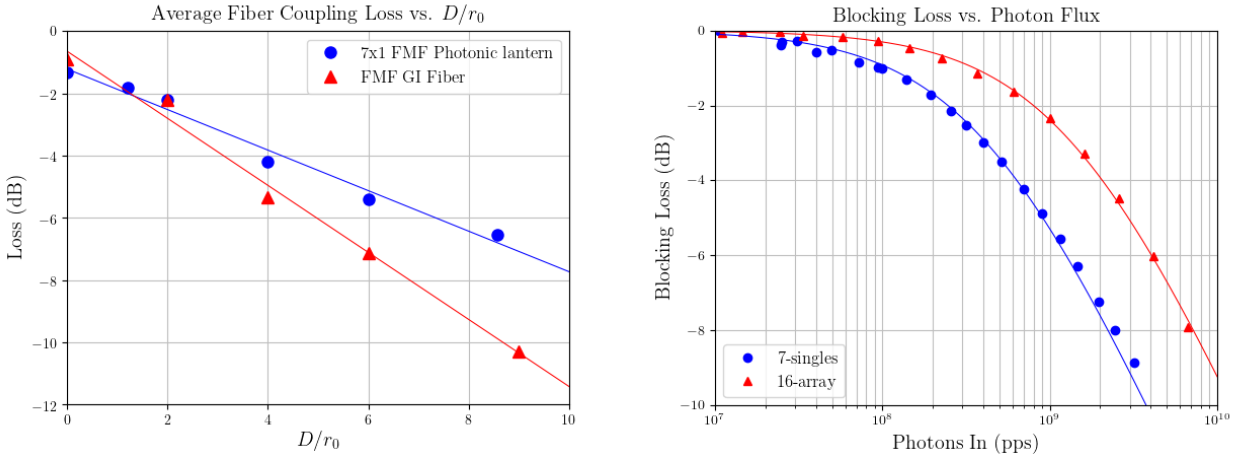

(a) (b)

Figure 8: (a) Average measured fiber interconnect coupling loss for best NA versus increasing turbulence, with linear fits $y_{PL}(x) = -0.652x - 1.214$, $R^2 = 0.981$, $y_{FMF}(x) = -1.078x - 0.642$, $R^2 = 0.990$. (b) Aggregate SNSPD blocking loss versus incident photon flux. Solid lines are fits based on Poisson statistics,[22] with effective aggregate reset times $\tau_7 \approx 17$ ns and $\tau_{16} \approx 9.20$ ns.

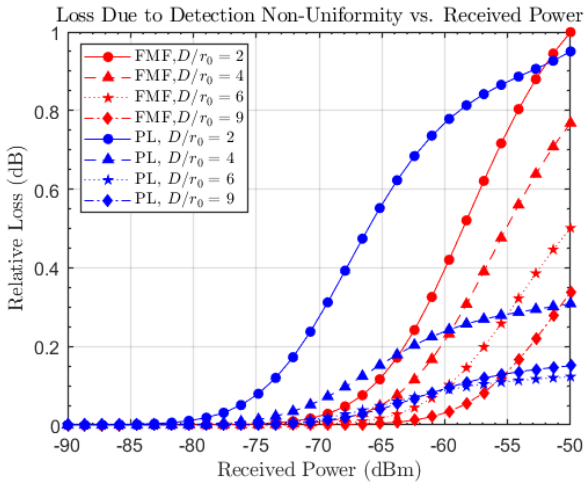

Figure 9: Additional detector blocking loss over a range of received power, due to the non-uniform distribution of incident light on the detectors.

Since detector blocking loss is depending on the incident photon flux, which is in turn dependent on the coupling loss of the fiber interconnect, we can combine the loss mechanisms, including the non-uniform detection distribution described in the previous section, to determine additional losses, and compare system performance vs. a range of received optical power. Received power in this case is referred to the input plane of either the photonic lantern or FMF, respectively. Figure 9 is an example of the additional blocking loss compared to an equally distributed input vs. received power for the two different configurations, and for $D/r_0 = \{2, 4, 6, 9\}$, with $\mathrm{NA}_{PL} = 0.064$ and $\mathrm{NA}_{FMF} = 0.16$. As input power increases, detector blocking loss increases and is further increased by the non-uniform distribution to the SNSPDs. However, as turbulence increases, coupling reduces, and the amount of incoming photons seen by the detectors reduces, hence loss decreases for the same input power. Regardless, the additional loss is less than 1.0 dB for a wide range of received power.

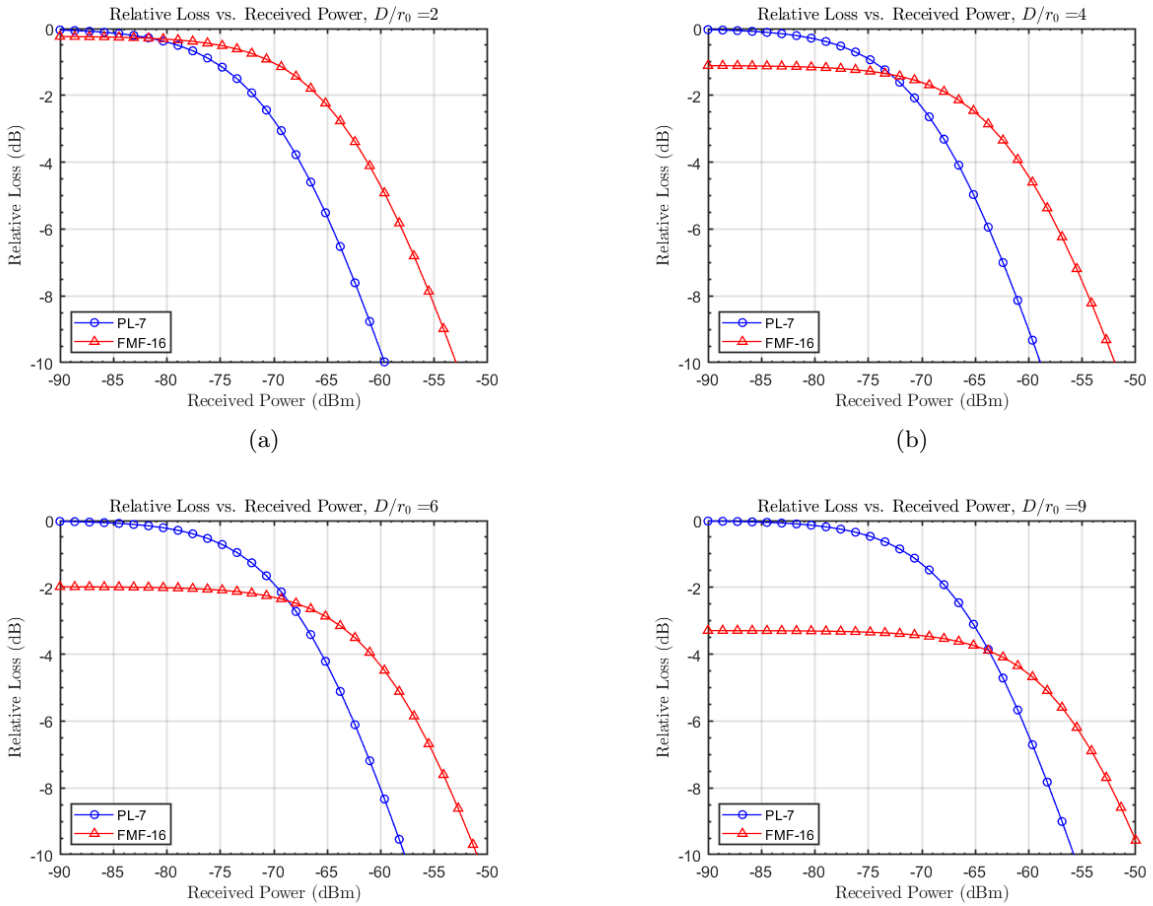

Figure 10: Fiber-detector receiver subsystem relative loss for (a) $D/r_0 = 2$, (b) $D/r_0 = 4$, (c) $D/r_0 = 6$, and (d) $D/r_0 = 9$.

Finally, we determine the relative loss between the photonic lantern, 7 single-element SNSPD system, and the FMF, SNSPD array system as a function of received power. The results of this comparison are shown in Figure 10, where we normalize to the coupling loss of the photonic lantern. Generally, the FMF system has more loss for lower received power, P_{RX}, and for all D/r_0 where detector blocking losses are negligible and coupling loss dominates. As P_{RX} increases, blocking losses increase prominently for the photonic lantern system, hence there is a cross-over P_{RX} where the relative coupling loss and blocking losses between the two systems are equal. The table depicted in Figure 11 summarizes the cross-over P_{RX}, and the relative loss below this point for the four different D/r_0.

D/r0	Relative Loss (dB)	P_{RX} (dBm)
2	0.20	-81.31
4	1.08	-72.82
6	1.96	-68.78
9	3.28	-63.53

Figure 11: Cross-over P_{RX} and relative loss for different D/r_0.

5. LINK PERFORMANCE ESTIMATION

With the fiber-detector subsystem losses accounted for as described in Section 4, we estimate the potential of the two receiver architectures to achieve various data rates. To do so we select from the modulation parameters defined by CCSDS HPE, the PPM order $M = \{4, 8, 16, 32, 64, 128, 256\}$, code rate, $CR = \{1/3, 1/2, 2/3\}$, and slot width $T_s = \{0.5, 1, 2, 4, 8, 16, 32\}$ ns, corresponding to data rates from $\approx$ 260 kbps - 533 Mbps. We assume a constant background noise of $K_b = 0.01$ ph/slot, and an additional implementation loss of $IL_{PL} \approx 0.3$ dB for the photonic lantern-single element SNSPD system, and $IL_{FMF} \approx 1.2$ dB for the FMF-SNSPD array system which accounts for SNSPD timing jitter loss and FPGA implementation.[9] For a given input power, P_{RX}, and turbulence level, D/r_0, for the different receiver concepts we calculate the total coupling loss from the linear relationship noted in Figure 8a, and use the average of the three non-uniform splitting ratio results shown in Section 4 to determine the input photon flux per detector. Further, assuming a per-detector detection efficiency of 70%, and based on the average SNSPD reset times, we can estimate the average count rate per detector, and then sum to find the total output count rate. From the modulation parameters we determine Ks/M, the number of detected signal photons per slot, and compare to SCPPM BER performance at a level of 10^{-6}. Assuming at least 2 dB of margin, we can determine the required P_{RX}. Figure 12 shows the results for $D/r_0 = 9$.

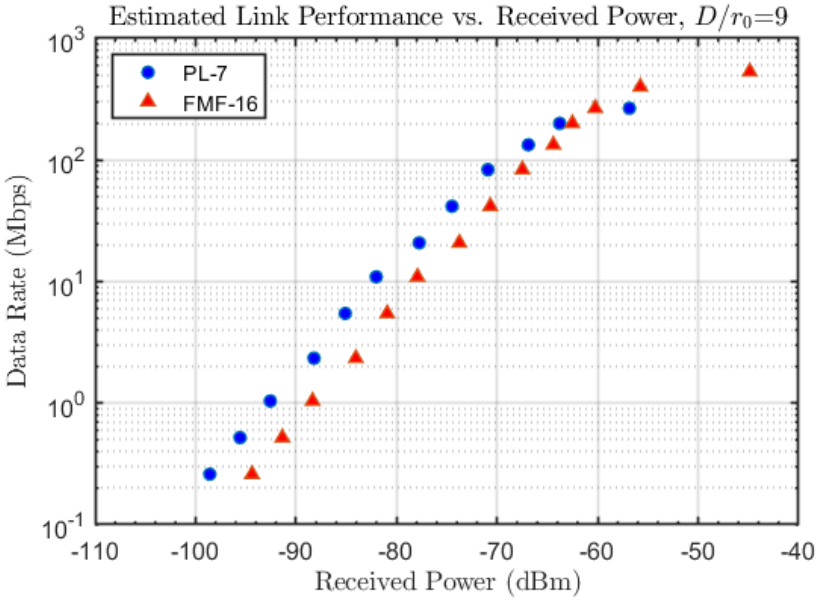

Figure 12: Data rate vs. received power for $D/r_0 = 9$.

From Figure 12 we can see the achievable data rates for the two architectures, and how the system losses translate into received power requirements for a given data rate. The photonic lantern system performs nearly 5 dB better, 3.62 dB relative loss + 1.2 dB implementation loss, for data rates up to about 100 Mbps. For higher data rates, the received power requirement increases and the gap between the two systems decreases, as described in Section 4, with the cross-over point at $P_{RX} \approx -63.5$ dBm corresponding to a data rate of about 200 Mbps. The losses on the photonic lantern, single SNSPD system increase quickly at higher input power, hence the achievable data rate tops out at the 267 Mbps level. The FMF-SNSPD array system has the potential to reach 400 Mbps and possibly 533 Mbps, although marginal reduction in the SNSPD reset time by a few ns may be needed. Additionally, given the relatively simple design and use of commercial components, with additional detectors and wavelength multiplexing, it may be possible to increase data rates into the several Gbps with minimal modification.

6. SUMMARY

We have characterized the main loss mechanisms for two fiber-detector subsystem architectures as part of a photon-counting optical receiver system designed for compatibility with the CCSDS HPE optical communications standard. Losses due to coupling in atmospheric turbulence, single-photon detector blocking loss, and losses due to non-uniform signal splitting between the detectors was quantified, for a range of input power and various D/r_0. Turbulence levels up to $D/r_0 = 9$ were evaluated for each subsystem, which correspond to possible conditions at the NASA LCOT where NASA GRC intends to demonstrate the receiver in collaboration with NASA Goddard Space Flight Center (GSFC) in support of Artemis-2. With optimal coupling, the receiver concept based on a FMF photonic lantern with 7 single-element SNSPDs has lower total losses for lower data rates and lower powers, but for rates above 200 Mbps the single FMF-SNSPD array system outperforms and can potentially achieve data rates up to 533 Mbps.

ACKNOWLEDGMENTS

The authors would like to acknowledge the support by the NASA Space Communications and Navigation (SCaN) program and the Glenn Research Center Communications & Intelligent Systems Division.

REFERENCES

[1] Moison, B. and Hamkins, J., "Coded modulation for the deep-space optical channel: Serially concatenated pulse position modulation," *The Interplanetary Network Progress Report* **42**(161) (2005).

[2] Consultative Committee for Space Data Systems (CCSDS), *Optical Communications Coding and Synchronization Recommended Standard, 142.0-B-1 Blue Book* (2019).

[3] Robinson, B. S., Shih, T., Khatri, F. I., Boroson, D. M., Burnside, J. W., Guldner, O., Constantine, S., Torres, J., Yarnall, T. M., DeVoe, C. E., Hubbard, W., Geisler, D. J., Stevens, M. L., Mikulina, O., Spellmeyer, N. W., Wang, J. P., Butler, R., Hogan, M., King, T., and Seas, A., "Laser communications for human space exploration in cislunar space: ILLUMA-T and O2O," in [*Free-Space Laser Communication and Atmospheric Propagation XXX*], Hemmati, H. and Boroson, D. M., eds., **10524**, 231 – 235, International Society for Optics and Photonics, SPIE (2018).

[4] Biswas, A., Srinivasan, M., Piazzolla, S., and Hoppe, D., "Deep space optical communications," in [*Free-Space Laser Communication and Atmospheric Propagation XXX*], Hemmati, H. and Boroson, D. M., eds., **10524**, 242 – 252, International Society for Optics and Photonics, SPIE (2018).

[5] Oh, D. Y., Collins, S., Goebel, D., Hart, B., Lantoine, G., Snyder, S., Whiffen, G., Elkins-Tanton, L., Lord, P., Pirkl, Z., and Rotlisburger, L., "Development of the Psyche Mission for NASA's Discovery Program," in [*35th International Electric Propulsion Conference*], Georgia Institute of Technology (October 2017).

[6] Tedder, S. A., Vyhnalek, B. E., Leon-Saval, S., Betters, C., Floyd, B., Staffa, J., and Lafon, R., "Single-mode fiber and few-mode fiber photonic lanterns performance evaluated for use in a scalable real-time photon counting ground receiver," in [*Free-Space Laser Communications XXXI*], Hemmati, H. and Boroson, D. M., eds., **10910**, 69 – 78, International Society for Optics and Photonics, SPIE (2019).

[7] Tedder, S. A., Floyd, B., Chahine, Y. K., Croop, B., Vyhnalek, B. E., Betters, C., and Leon-Saval, S. G., "Measurements of few-mode fiber photonic lanterns in emulated atmospheric conditions for a low earth orbit space to ground optical communication receiver application," in [*Free-Space Laser Communications XXXII*], Hemmati, H. and Boroson, D. M., eds., **11272**, 112720U, International Society for Optics and Photonics, SPIE (2020).

[8] Tedder, S. A., Vyhnalek, B. E., Chahine, Y. K., and Floyd, B., "Insertion loss of a multi-plane light conversion device with few mode fiber outputs under atmospheric conditions," in [*Free-Space Laser Communications XXXIV*], Hemmati, H. and Robinson, B. S., eds., **11993**, 1199305, International Society for Optics and Photonics, SPIE (2022).

[9] Downey, J. N., Tedder, S. A., Vyhnalek, B. E., Lantz, N. C., Marsden, M. A., Simon, W. P., Bizon, T. P., and Zeleznikar, D. J., "A real-time optical ground receiver for photon starved environments," in [*Free-Space Laser Communications XXXV*], International Society for Optics and Photonics, SPIE (2023).

[10] You, L., "Superconducting nanowire single-photon detectors for quantum information," *Nanophotonics* **9**(9), 2673–2692 (2020).

[11] Vyhnalek, B. E., Tedder, S. A., Katz, E. J., and Nappier, J. M., "Few-mode fiber coupled superconducting nanowire single-photon detectors for photon efficient optical communications," in [*Free-Space Laser Communications XXXI*], Hemmati, H. and Boroson, D. M., eds., **10910**, 62 – 75, International Society for Optics and Photonics, SPIE (2019).

[12] Vyhnalek, B. E., Downey, J. N., and Tedder, S. A., "Single-photon counting detector scalability for high photon efficiency optical communications links," in [*Free-Space Laser Communications XXXII*], Hemmati, H. and Boroson, D. M., eds., **11272**, 112721A, International Society for Optics and Photonics, SPIE (2020).

[13] Sillard, P., Molin, D., Bigot-Astruc, M., Maerten, H., Ras, D. V., and Achten, F., "Low-dmgd 6-lp-mode fiber," in [*Optical Fiber Communication Conference*], *Optical Fiber Communication Conference* , M3F.2, Optica Publishing Group (2014).

[14] Rambo, T. M., Conover, A. R., and Miller, A. J., "16-element superconducting nanowire single-photon detector for gigahertz counting at 1550-nm," (2021).

[15] Robinson, B. S., Boroson, D. M., Burianek, D. A., Murphy, D. V., Khatri, F. I., Burnside, J. W., Kansky, J. E., Biswas, A., Sodnik, Z., and Cornwell, D. M., "The NASA lunar laser communication demonstration - successful high-rate laser communications to and from the moon," in [*AIAA - SpaceOps 2014*], (2014).

[16] Vyhnalek, B. E., Tedder, S. A., and Nappier, J. M., "Performance and characterization of a modular superconducting nanowire single photon detector system for space-to-Earth optical communications links," in [*Free-Space Laser Communication and Atmospheric Propagation XXX*], Hemmati, H. and Boroson, D. M., eds., **10524**, 369 – 377, International Society for Optics and Photonics, SPIE (2018).

[17] Chahine, Y. K., Tedder, S. A., Floyd, B., and Vyhnalek, B. E., "Verification of the mode fidelity and fried parameter for optical turbulence generated by a spatial light modulator," *Opt. Continuum* **1**, 2112–2126 (Oct 2022).

[18] Sarah A. Tedder, Y. K. C., "Folded optical design for high fidelity atmospheric emulation with a spatial light modulator," in [*Free-Space Laser Communications XXXV*], International Society for Optics and Photonics, SPIE (2023).

[19] Chahine, Y. K., Tedder, S. A., Vyhnalek, B. E., and Wroblewski, A. C., "Beam propagation through atmospheric turbulence using an altitude-dependent structure profile with non-uniformly distributed phase screens," in [*Free-Space Laser Communications XXXII*], Hemmati, H. and Boroson, D. M., eds., **11272**, 1127215, International Society for Optics and Photonics, SPIE (2020).

[20] Chahine, Y. K., Tedder, S. A., Staffa, J., and Vyhnalek, B. E., "Optimal efficiency for passively coupling partially coherent light intomode-limited optical waveguides," *J. Opt. Soc. Am. A* **38**, 1732–1743 (Dec 2021).

[21] Lafon, R. E., Caroglanian, A., Safavi, H., Desch, N., Wu, V. C., Buenfil, M., Thompson, P. L., Merritt, S., Hall, S., Garon, H., Paulson, D. A., Speer, J. V., Wilson, M., Miller, R., Haas, T., Trout, B., Mason, R., Hengemihle, J., and Guzek, J. A., "A flexible low-cost optical communications ground terminal at NASA Goddard Space Flight Center," in [*Free-Space Laser Communications XXXIII*], Hemmati, H. and Boroson, D. M., eds., **11678**, 1167806, International Society for Optics and Photonics, SPIE (2021).

[22] Schätzel, K., Kalström, R., Stampa, B., and Ahrens, J., "Correction of detection-system dead-time effects on photon-correlation functions," *J. Opt. Soc. Am. B* **6**, 937–947 (May 1989).